EXCITATION OF ION-CYCLOTRON HARMONIC WAVES IN LOWER-HYBRID HEATING*

E. Villalón

PFC/JA-80-19 September 1980

* Work supported by the U.S. Department of Energy Contract ET78-S-02-4682.

EXCITATION OF ION-CYCLOTRON HARMONIC WAVES IN LOWER-HYBRID HEATING

E. VILLALÓN

Plasma Fusion Center

Massachusetts Institute of Technology

Cambridge, Massachusetts 02139.

Abstract

The parametric excitation of ion-cyclotron waves by lower-hybrid pump field is studied assuming that the magnitude of the pump is constant. The spatial amplification factor is calculated including the wavenumber mismatch as produced by the plasma density gradient, and the linear damping rates of the excited ion-cyclotron and sideband waves. The analysis is applied to plasma edge parameters relevant to the JFT2 heating experiment. It is found that ion-cyclotron harmonic modes are excited depending on pump frequency and plasma density. These modes are shown to have finite damping rates. The parallel refractive indices n_{1z} of the excited sideband fields are found to be always larger than that of the driven pump field. Transition to quasi-mode decay is observed for the largest possible excited n_{1z}, either by decreasing the pump frequency or by increasing the applied Rf-power.

I. INTRODUCTION

Lower-hybrid heating is one of the most attractive techniques for supplementary heating of tokamak plasmas because of its engineering feasibility. But it requires a high degree of physical understanding on how the driven Rf-fields coupled with the plasma. This is because at the Rf-power levels which are needed for significant plasma heating, parametric instabilities, driven by the applied lower-hybrid fields, will inevitably occur [1]. One of the most important problems in lower-hybrid heating is the energy penetration in the plasma. Parametric excitations can change the wavenumber spectra of the fields entering the plasma [2], which may lead to an unwanted surface heating and pump depletion near the plasma edge. They may also deposit a certain amount of energy near the edge by exciting low frequency waves (such as ion-cyclotron harmonic waves) with finite linear damping rates.

There are a variety of parametric excitations that may occur during lower-hybrid heating. Among them, the decay into electrostatic ion-cyclotron harmonic and lower-hybrid sideband waves [1,3,4] is one of the most important in this range of frequency. In fact, decay spectra was recently observed in the JFT2 heating experiment [5]. It was discussed that the existance of this decay spectra is responsible for the blockade of a certain amount of the input power near the plasma edge. Several others heating experiments [6] have also observed the presence of such excitations. It is of interest to understand how they physically act to prevent power penetration in the plasma and also, to know the plasma configuration and the characteristics of the driven fields which more likely lead to the development of the instability. To our knowledge, these questions have not yet received a satisfactory answer. It is this deficiency that this paper attempts to remedy.

Near the edge of a tokamak the plasma density gradient is usually very strong. This has been shown [7,8] to be important to reduce the level of growth of the instability by detuning the resonant nature of the parametric decay. In addition, the excited ion-cyclotron waves may be damped either by electrons or ions, which also partially depress the resonant excitation. In a previous

work [9], we studied how these two effects act together to prevent the development of the resonant decay, assuming a constant pump electric field and a linear profile for the wavenumber mismatch as produced by the plasma density gradient; the thresholds and growth rates were calculated within the WKB approximation. It is this study that we apply in this paper to the particular decay into ion-cyclotron and lower-hybrid waves. Numerical calculations are carried out for plasma edge parameters relevant to the JFT2 experiment. These calculations show that the wavenumber mismatch and the linear damping rates of the excited waves play a decisive role to decide whether the resonant decay takes place or not. In fact, their values are usually as large as the instability rarely grow in the entire pump region, but rather saturates before reaching the extremes of the pump propagation cone. Because of this, we shall not consider the excitation of temporally growing normal modes, since they are very unlikely to develop under such unfavorable circumstances. We only consider the excitation of spatially amplified solutions.

The organization of the paper is as follows. In Sec. II we present the dispersion relations for the two lower-hybrid and the excited ion-cyclotron harmonic waves. The linear damping rates are obtained as functions of the wavenumbers and frequencies of the excited waves. We take $\omega_2/(|k_{2z}|v_{Te})$, where the subscript 2 stands for the ion-cyclotron wave, as a free parameter which has to be much smaller than one for the wave not to be strongly damped by electrons. The frequency and perpendicular wavenumber of the low frequency mode are chosen, for each excited harmonic, such that they satisfy the dispersion relation and minimize ion damping. Others free parameters (i.e., frequency and wavenumber of the excited sideband field) follow from the lower-hybrid dispersion relation and from the resonant matching conditions. In Sec. III, we present the equations that describe the parametric decay assuming that the pump field is constant over the region of resonant interaction. The amplification factor is found within the WKB approximation as function of the wavenumber mismatch and linear damping rates, and it is maximized with respect to angular dependences. In Sec. IV, we present the numerical examples. We show that given a certain value of the plasma density and density gradient, ion-cyclotron waves can be excited for a limited range in pump frequency. The higher excited harmonics are found to suffer the strongest damping due to

both electrons and ions. The mismatch is the strongest for the lowest excited harmonics. The parallel refractive index n_{1z} for the excited sideband field is shown to be very large, because the amplification factor Γ is the largest for the highest possible excited n_{1z}. The scaling of Γ with respect to plasma density and applied input power is also discussed in this section.

Finally, it should be noted that because we do not carry out nonlinear calculations that take into account pump depletion; we cannot give an estimation on the amount of energy that has been transferred to the excited waves. Our calculations show that these parametric excitations can really be very relevant in lower-hybrid heating and that, if they occur, it is inevitable that appreciable amount of the applied power is deposited on the particles at the edge. One of the main purposes of this paper is to study how amplification scales with respect to plasma density, pump frequency, and applied Rf-power, since we believe that this is essential to understand and, subsequently, to control the ocurrence of this resonant decay.

II. BASIC EQUATIONS

We consider a plasma slab; the x-coordinate lies along the direction of variation of the plasma density and the z-coordinate lies along the direction of propagation of the constant magnetic field $\vec{B}_0$. A lower-hybrid pump electric field $(\omega_0, \vec{k}_0)$, is assumed to parametrically decay into a sideband lower-hybrid field $(\omega_1, \vec{k}_1)$, and an ion-cyclotron harmonic mode $(\omega_2, \vec{k}_2)$. The three waves are described by their amplitudes,

$$A_i = a_i(x, z, t) \exp[i(-\omega_i t + k_{iz} z + k_{iy} y) + i \int^x k_{ix}(x') \, dx'] . \qquad (1)$$

We assume that $k_{0y} = 0$ and that a_0 is constant in time. The waves satisfy the matching conditions: $k_{0z} = k_{1z} + k_{2z}$, $k_{2y} = -k_{1y}$, and $\omega_0 - \omega_1 - \omega_2 = 0$. The perpendicular wavenumbers $k_{i\perp} = (k_{ix}^2 + k_{iy}^2)^{1/2}$ are determined from the local dispersion relation for each of the waves in the inhomogeneous plasma as we shall specify next. Due to the plasma density gradient, the mismatch between the x-components of the wavenumbers $\Delta k = k_{0x} - k_{1x} - k_{2x}$, depends on the inhomogeneity coordinate x. This phase mismatch is increasingly detuning the resonant interaction between the three waves, as it deviates from its corresponding constant value in a homogeneous plasma.

For spatially amplified solutions, we require that the dependence of the amplitudes a_i $(i = 1,2)$ on time be given by $\exp(i \, \Delta\omega \, t)$, where $\Delta\omega$ will be defined in Sec. III.

A. Ion-cyclotron harmonic waves

Let us denote by p the number of the excited cyclotron harmonic $(p = 1,2,3,...)$. The low frequency mode approximately satisfy a dispersion relation of the form $D(\omega_2, \vec{k}_2) \simeq 0$. Quite generally this dispersion relation is,

$$D(\omega_2, \vec{k}_2) = \frac{1}{k_2^2 \lambda_{De}^2} [1 + \frac{\omega_2}{\sqrt{2}|k_{2z}|v_{Te}} Z_R(\frac{\omega_2}{\sqrt{2}|k_{2z}|v_{Te}})]$$

$$+\frac{1}{k_2^2\lambda_{Di}^2}\Big[1+\frac{\omega_2}{\sqrt{2}|k_{2z}|v_{Ti}}\sum_{n=p-\ell}^{n=p+\ell}\Lambda_n(k_{2\perp}^2\,\rho_i^2)\,Z_R\Big(\frac{\omega_2}{\sqrt{2}|k_{2z}|v_{Ti}}(1-n\frac{\Omega_i}{\omega_2})\Big)\Big] \qquad (2)$$

where we assume that $k_2^2\lambda_{De}^2 \gg 1$, and where $\rho_i = v_{Ti}/\Omega_i$; $T_{e,i}$ are the electron (ion) plasma temperatures, $\Lambda_n = \exp(-k_{2\perp}^2\rho_i^2)\,I_n(k_{2\perp}^2\rho_i^2)$, and Z_R denotes the real part of the plasma dispersion function. The summation contains those harmonics, close to the excited harmonic $n = p$, that give an appreciable contribution to the dispersion relation; (in specific calculations as the ones presented in Sec. IV, we find that ℓ is equal to 2 or 3)

We take the ratio $\omega_2/(|k_{2\,z}|v_{Te})$ as a free parameter which has to be always smaller than one so that the low frequency mode is not strongly Landau damped by electrons. The frequency ω_2 and the perpendicular wavenumber $k_{2\perp}$ are to be determined from the dispersion relation $D(\omega_2, \vec{k}_2) \simeq 0$ as proceeds. First we fix a value of ω_2 close to $p\Omega_i$ and such that satisfy

$$\frac{\omega_2}{\sqrt{2}|k_{2z}|v_{Ti}}\,|1-n\frac{\Omega_i}{\omega_2}| > 1,$$

with $n = p$, $p\pm1$ (the exact range of variation of ω_2 will be specified later in Eq. (4)). The perpendicular wavenumber is obtained as function of ω_2 and $\omega_2/|k_{2z}|$ solving for

$$\Lambda_p(k_{2\perp}^2\rho_i^2) = -\frac{T_i}{T_e}\;\frac{1+T_e/T_i+\omega_2/(\sqrt{2}|k_{2z}|v_{Te})\,Z_R\,[\omega_2/(\sqrt{2}|k_{2z}|v_{Te})]}{\omega_2/(\sqrt{2}|k_{2z}|v_{Ti})\,Z_R[\omega_2/(\sqrt{2}|k_{2z}|v_{Ti})\,(1-p\,\Omega_i/\omega_2)]}. \qquad (3)$$

The left-hand side of Eq. (3) is always positive. The right-hand side is, for $T_e \simeq T_i$, either positive or negative depending on whether ω_2 is either greater or smaller than $p\Omega_i$. Furthermore, the Bessel function is bounded to a maximum value that becomes smaller as the order of the excited harmonic p increases. Let us call β_m the value of $k_{2\perp}\rho_i$ for which the Bessel function is maximal. We have that β_m becomes larger with increasing p; for instance, for $p = 1$ we find that $\beta_m = 1.54$ and $\Lambda_1(\beta_m) = 0.22$, for $p = 3$ $\beta_m = 9.53$ and $\Lambda_3(\beta_m) = 0.08$, for $p = 5$ $\beta_m = 25.51$ and $\Lambda_5(\beta_m) = 0.05$. Thus, as the order of the harmonic increases the argument of the Z-function in the denominator of Eq. (3) has to be closer to one so that the right-hand side does not exceed the maximum value that the Bessel function can reach at $k_{2\perp}\rho_i = \beta_m$. All this imposes restrictions on ω_2 as it has to be always greater than $p\Omega_i$, in order to be able to solve Eq. (3) for a real $k_{2\perp}$. In addition, if α_m is the

frequency that solves Eq. (3) for $k_{2\perp}\rho_i = \beta_m$, we need also to require for ω_2 to be smaller than or equal to α_m.

We call ω_m the minimum value between α_m and

$$(p+1)\Omega_i \frac{\omega_2/(\sqrt{2}|k_{2z}|v_{Ti})}{\omega_2/(\sqrt{2}|k_{2z}|v_{Ti})+1}.$$

The frequency ω_2 is to be chosen within the range

$$p\Omega_i \frac{\omega_2/(\sqrt{2}|k_{2z}|v_{Ti})}{\omega_2/(\sqrt{2}|k_{2z}|v_{Ti})-1} < \omega_2 < \omega_m. \tag{4}$$

It should be noted that in Eq. (3) we have neglected the contribution of all other harmonics different from the excited harmonic $n = p$. This, we find, can always be done for ω_2 inside the interval in Eq. (4), because the contribution to the dispersion relation of equidistant harmonics such as $p-1$ and $p+1$, have always opposite signs. Thus, when they are added together the result is very small, and the dispersion relation in Eq. (2) is always approximately satisfied. To find the exact value of ω_2 within the interval in Eq. (4), we require minimum damping for the low frequency mode, i.e., we want the following expression to be minimal with respect to ω_2 for $k_{2\perp}$ as given in Eq. (3),

$$\Lambda_p(k_{2\perp}^2\rho_i^2)\exp[-(\frac{\omega_2 - p\Omega_i}{\sqrt{2}k_{2z}v_{Ti}})^2] + \Lambda_{p+1}(k_{2\perp}^2\rho_i^2)\exp[-(\frac{\omega_2-(p+1)\Omega_i}{\sqrt{2}k_{2z}v_{Ti}})^2].$$

In the numerical calculations we find that this expression is minimal for $k_{2\perp}\rho_i \simeq \beta_m$, which corresponds to a frequency of the order of $(p+0.5)\Omega_i$.

The low frequency mode may be slightly damped either by electrons or ions. The linear damping rate is found to be,

$$\frac{\gamma_2}{\omega_2} = \sqrt{\pi}\,\frac{\sqrt{2}|k_{2z}|v_{Ti}}{\omega_2}\,\frac{\omega_2}{\Omega_i}\,\frac{1}{S}\Big(\frac{T_i}{T_e}\frac{v_{Ti}}{v_{Te}}\exp(-\frac{\omega_2^2}{2k_{2z}^2v_{Te}^2})$$

$$+\Lambda_p(k_{2\perp}^2\rho_i^2)\exp[-(\frac{\omega_2-p\Omega_i}{\sqrt{2}k_{2z}v_{Ti}})^2] + \Lambda_{p+1}(k_{2\perp}^2\rho_i^2)\exp[-(\frac{\omega_2-(p+1)\Omega_i}{\sqrt{2}k_{2z}v_{Ti}})^2]\Big) \tag{5}$$

where

$$S = \sum_{n=p-\ell}^{n=p+\ell} n\,\Lambda_n(k_{2\perp}^2\rho_i^2)\,Z_R'\left(\frac{\omega_2 - n\Omega_i}{\sqrt{2}|k_{2z}|v_{Ti}}\right)$$

and where Z_R' denotes the derivative of the real part of the plasma dispersion function with respect to its argument.

The perpendicular component of the group velocity is given by

$$\frac{v_{2\perp}}{v_{Ti}} = -2\,k_{2\perp}\rho_i\,\frac{\sqrt{2}|k_{2z}|v_{Ti}}{\omega_2}\left(\frac{\omega_2}{\Omega_i}\right)^2\frac{R}{S} \tag{6}$$

where

$$R = \sum_{n=p-\ell}^{n=p+\ell} \Lambda_n'(k_{2\perp}^2\rho_i^2)\,Z_R\left(\frac{\omega_2 - n\Omega_i}{\sqrt{2}|k_{2z}|v_{Ti}}\right)$$

and where Λ_n' denotes the derivative of Λ_n with respect to its argument. Since $\omega_2/(|k_{2z}|v_{Te}) \ll 1$, and $|\omega_2 - n\Omega_i|/(|k_{2z}|v_{Ti}) \gg 1$, we may expand the Z-functions in Eq. (2), for small and large argument, respectively. The result is that $D(\omega_2, \vec{k}_2)$ is approximately independent of k_{2z}, which implies that the group velocity component along the z-direction is approximately equal to zero. As Eq. (2) does not depend on the plasma density, the perpendicular wavenumber $k_{2\perp}$ and group velocity $v_{2\perp}$ are constants independent of x.

B. Lower-hybrid waves

For the two lower-hybrid waves, we have ($i = 0, 1$)

$$k_{iz}^2 K_{i\parallel}(x) + k_{i\perp}^2 K_{i\perp}(x) = 0 \tag{7}$$

where $K_{i\parallel} = 1 - \omega_{pe}^2(x)/\omega_i^2$, and $K_{i\perp} = 1 + \omega_{pe}^2(x)/\Omega_e^2 - \omega_{pi}^2(x)/\omega_i^2$. The lower-hybrid pump field is assumed to have a finite spatial extent w along the z-coordinate; it propagates in the plasma with group velocities,

$$v_{0z} = \frac{1}{n_{0z}}\,\frac{c}{1 + \omega_{pe}^2/\Omega_e^2}\,K_{0\perp} \tag{8a}$$

$$v_{0\perp} = -\frac{1}{n_{0z}} \frac{c}{1 + \omega_{pe}^2/\Omega_e^2} \left(\frac{K_{0\perp}^3}{-K_{0m}}\right)^{1/2} \tag{8b}$$

as taken along and perpendicular to $\vec{B}_0$ (note that as $k_{0y} = 0$, we have $v_{0\perp} = v_{0x}$); where c denotes the velocity of light, and $n_{0z} = ck_{0z}/\omega_0$ is assumed to be always positive. The slowly varying pump amplitude $a_0(x, z)$ is taken constant over the region where the pump extends:

$$-\frac{w}{2} \le z - \int_r^x \frac{v_{0z}(x')}{v_{0x}(x')}\, dx' \le \frac{w}{2},$$

and zero outside this region, where r is the slab half-width. As the pump field is propagating toward the plasma center (i.e., from $x = r$ toward $x = 0$), we have that $v_{0x} < 0$.

The sideband lower-hybrid electric field exists initially in the plasma at the level of thermal fluctuations; it propagates with group velocities which are given by substituting the subscript 0 by 1, in Eqs. (8). The thermal source may interact with the pump at a certain point inside the pump region, and then the three waves parametric instability may develop. The sideband field may be slightly damped by electrons. The linear damping rate is

$$\frac{\gamma_1}{\omega_1} = \sqrt{\pi} \left(\frac{\omega_1}{\sqrt{2}|k_{1z}|v_{Te}}\right)^3 \left(\frac{\omega_{pe}\omega_{\ell h} v_{1\perp}}{\omega_1 \omega_{pi} v_{1z}}\right)^2 \exp\left(-\frac{\omega_1^2}{2\, k_{1z}^2\, v_{Te}^2}\right) \tag{9}$$

where $\omega_{\ell h} = \omega_{pi}/(1 + \omega_{pe}^2/\Omega_e^2)^{1/2}$.

By imposing the matching conditions, the parallel refractive index $n_{1z} = ck_{1z}/\omega_1$ of the excited sideband field is given by

$$\frac{\omega_1}{k_{1z} v_{Te}} = \frac{\omega_2}{k_{2z} v_{Te}} \frac{1 - \omega_2/\omega_0}{\dfrac{\omega_2/k_{2z} v_{Te}}{\omega_0/k_{0z} v_{Te}} - \omega_2/\omega_0}. \tag{10}$$

For $\omega_2/k_{2z} > 0$, n_{1z} can be either positive or negative depending on whether $\omega_2/(k_{2z} v_{Te})$ is either greater or smaller than $d = (\omega_2/\omega_0)\, \omega_0/(k_{0z} v_{Te})$, respectively. As $\omega_2/(k_{2z} v_{Te})$ becomes closer to d, n_{1z} tends to zero. For $\omega_2/k_{2z} < 0$, n_{1z} is always positive and will never be smaller than n_{0z}. Given a fixed value of $\omega_2/|k_{2z}|$ and of ω_2/ω_0, we find that the corresponding n_{1z} is larger in magnitude if ω_2/k_{2z} is negative than if it is positive.

It should be noted that the group velocity components of the pump and sideband waves, and the pump amplitude, depend on the inhomogeneity coordinate x. Nevertheless, the most significant effect of the plasma density gradient is to produce a mismatch between the x component of the wavenumbers, which may significantly reduce the level of growth of the instability. All other quantities that do not contribute to the phase mismatch will be assumed constant over the region of resonant interaction.

III. THE MAXIMUM AMPLIFICATION FACTOR

The spatial evolution of the instability is given by the following set of coupled equations [10]

$$(i\Delta\omega + \gamma_1 + v_{1x}\frac{\partial}{\partial x} + v_{1z}\frac{\partial}{\partial z})a_1 = \gamma_0 a_2^* \exp[i\int^x \Delta k(x')\,dx'], \tag{11a}$$

$$(i\Delta\omega + \gamma_2 + v_{2x}\frac{\partial}{\partial x} + v_{2z}\frac{\partial}{\partial z})a_2 = \gamma_0 a_1^* \exp[i\int^x \Delta k(x')\,dx']. \tag{11b}$$

Within the E x B approximation the coupling coefficient is [1-4]

$$\frac{\gamma_0}{\sqrt{\omega_1\omega_2}} = \frac{E_0\,\omega_{lh}}{2B_0\,c_s\,\omega_0}\,\frac{|k_{2z}|v_{Ti}}{\omega_2}\,\sin(\phi)\left(\frac{T_i\,\omega_2}{T_e\,\Omega_i\,|S|}\right)^{1/2}\left(1 + \frac{\omega_2}{\sqrt{2}|k_{2z}|v_{Te}}\,Z_R\!\left(\frac{\omega_2}{\sqrt{2}|k_{2z}|v_{Te}}\right)\right) \tag{12a}$$

where E_0 is the constant pump electric field which is related to a_0 as, $E_0 = a_0/2\;\omega_{lh}/\omega_{pi}\;\sqrt{\omega_0/2}$; c_s is the sound speed, and $\sin(\phi) = k_{1y}/k_{1\perp}$. The pump electric field is given as a function of the power density p_d (i. e., the total power divided by the waveguide widths w) as follows,

$$E_0 = \left(\frac{2}{c\,\varepsilon_0}\,p_d\,n_{0z}\sqrt{\frac{-K_{0\parallel}}{K_{0\perp}^3}}\right)^{1/2}. \tag{12b}$$

Let us call $\bar{z} = (v_{0z}\,z + v_{0x}\,x)/v_0$ and $\bar{x} = (v_{0z}\,x - v_{0x}\,z)/v_0$ (where $v_0 = (v_{0x}^2 + v_{0z}^2)^{1/2}$), the coordinates that lie respectively along and perpendicular to the pump propagation cone. We define a new coordinate system as,

$$\begin{aligned} \xi &= \rho\,\bar{x} \\ z_f &= \bar{z} - \alpha\,\bar{x} \end{aligned} \tag{13}$$

where $\alpha = (v_{1\bar{z}} - v_{2\bar{z}})/(v_{1\bar{x}} - v_{2\bar{x}})$, and $\rho = (v_{0z} + \alpha\,v_{0x})/v_0$. It has been shown [11] that in terms of this system of coordinates, the two-dimensional resonant interaction in the coordinates (x, z) becomes a one-dimensional one in the coordinate ξ:

$$(v_{1\xi}\,\frac{\partial}{\partial\xi} + \gamma_1 + i\Delta\omega)\,a_1(\xi, z_f) = \gamma_0\,a_2^*(\xi, z_f)\exp[i\int^{\xi}\Delta k(\xi' + \frac{v_{0x}}{v_0}\,z_f)\,d\xi'] \qquad (14a)$$

$$(v_{2\xi}\,\frac{\partial}{\partial\xi} + \gamma_2 + i\Delta\omega)\,a_2(\xi, z_f) = \gamma_0\,a_1^*(\xi, z_f)\exp[i\int^{\xi}\Delta k(\xi' + \frac{v_{0x}}{v_0}\,z_f)\,d\xi'] \qquad (14b)$$

This interaction is defined along lines of constant z_f, as shown in Fig. 1. The pump extension in ξ is $L = |\rho\ v_{0x}/v_{0z}|\ w$; where L is the distance that the pulse response (i.e., the line of constant z_f) covers in the inhomogeneity coordinate x, as it crosses the pump cone. The plasma density is assumed to obey the profile,

$$n(\xi) = n_0 + |\nabla n|\,\xi \qquad (15a)$$

where $|\nabla n|$ is the plasma density gradient (typically, $|\nabla n| \simeq 10^{12} - 10^{13}\ cm^{-4}$); n_0 is the plasma density at $\bar{x} = 0$, and $\bar{z} = z_f$ (or in the ξ coordinate at $\xi = 0$). The phase mismatch is assumed to be a linear function of ξ:

$$\Delta k(\xi) = K'\xi + \Delta k(0), \qquad (15b)$$

where $K' = [\Delta k(L/2) - \Delta k(-L/2)]/L$, and $\Delta k(0) = [\Delta k(L/2) + \Delta k(-L/2)]/2$. The mismatches at both extremes of the pump cone are to be evaluated at the local densities $n(\pm L/2)$ as given by Eq. (15a). All others quantities that do not contribute to the phase mismatch $\Delta k(\xi)$, are defined at the constant values that they take for $\xi = 0$ (i.e., at the central density n_0). Note that at $\xi = 0$ the mismatch is independent of K', so that the coupling between the waves is as in the corresponding homogeneous plasma which is defined by allowing K' go to zero.

We next define a new set of amplitudes $\hat{a}_1$, and $\hat{a}_2$ as

$$a_1 = \frac{\hat{a}_1}{\sqrt{|v_{1\xi}|}}\exp[-\frac{\xi}{2}(\frac{i\Delta\omega + \gamma_1}{v_{1\xi}} + \frac{i\Delta\omega + \gamma_2}{v_{2\xi}}) + \frac{i}{2}\int^{\xi}\Delta k(\xi')\,d\xi'] \qquad (16a)$$

$$a_2^* = \frac{\hat{a}_2}{\sqrt{|v_{2\xi}|}} \exp\left[-\frac{\xi}{2}\left(\frac{i\Delta\omega + \gamma_1}{v_{1\xi}} + \frac{i\Delta\omega + \gamma_2}{v_{2\xi}}\right) - \frac{i}{2}\int^{\xi} \Delta k(\xi')\, d\xi'\right] \tag{16b}$$

Substituting these expressions into Eqs. (14), we obtain

$$\left[\frac{1}{2}\beta(\xi) + \frac{\partial}{\partial\xi}\right]\hat{a}_1 = \mathrm{sgn}(v_{1\xi})\,\lambda_0\,\hat{a}_2 \tag{17a}$$

$$\left[-\frac{1}{2}\beta(\xi) + \frac{\partial}{\partial\xi}\right]\hat{a}_2 = \mathrm{sgn}(v_{2\xi})\,\lambda_0^*\,\hat{a}_1 \tag{17b}$$

where $\beta(\xi) = \lambda_D + iK'\xi$, $\lambda_D = \gamma_1/v_{1\xi} - \gamma_2/v_{2\xi}$, and $\lambda_0 = \gamma_0/\sqrt{|v_{1\xi}v_{2\xi}|}$. The frequency mismatch

$$\Delta\omega = -\frac{\Delta k(0)}{1/v_{1\xi} - 1/v_{2\xi}},$$

has been chosen so that the evolution of the instability, as given by Eqs. (17), becomes independent of any mismatch, either in frequency or phase, which is not strictly produced by the plasma inhomogeneities. The system of equations (17) have been studied for the case of a pump of infinite spatial extent in Ref. 7 . In Ref. 9 the coupled mode equations were studied assuming a constant pump of finite extent, which is the case that interests us now. The amplification factor was obtained using the WKB approximation and the procedure is briefly outlined in the Appendix.

Assuming that $\mathrm{sgn}(v_{1\xi}v_{2\xi}) > 0$, the amplification factor for the amplitudes a_i is found to be

$$\Gamma = -i\,\frac{2|\lambda_0|^2}{K'}\int_{c^*}^{c}(1+z^2)^{1/2}dz - \gamma_1\left|\frac{L}{v_{1\xi}}\right| - \gamma_2\left|\frac{L}{v_{2\xi}}\right| \tag{18a}$$

where $c = (\lambda_D + iK'L/2)/2|\lambda_0|$; and the integral is defined along the line $\mathrm{Re}(z) = \mathrm{Re}(c)$. By letting $|\lambda_D| \ll K'L$, Eq. (18a) becomes

$$\Gamma = \frac{|\lambda_0 L|}{2}\left[1 - \left(\frac{K'L}{4|\lambda_0|}\right)^2\right]^{1/2} + \frac{|\lambda_0|^2}{K'}\arcsin\left(\frac{K'L}{2|\lambda_0|}\left[1 - \left(\frac{K'L}{4|\lambda_0|}\right)^2\right]^{1/2}\right)$$

$$- \gamma_1\left|\frac{L}{v_{1\xi}}\right| - \gamma_2\left|\frac{L}{v_{2\xi}}\right|$$

within the limit $K', \gamma_i \to 0$ we find that Γ tends to $|\lambda_0 L|$ as presented in Ref. 12.

Equation (18a) is to be applied if the integration path does not intersect the anti-Stokes' lines departing from $z = \pm i$, which are defined in the Appendix. If this happens then the amplification factor is given by,

$$\Gamma = \pi \frac{|\Lambda_0|^2}{K'} - \gamma_1 |\frac{L}{v_{1\xi}}| - \gamma_2 |\frac{L}{v_{2\xi}}|. \tag{18b}$$

When $sgn(v_{1\xi} v_{2\xi}) < 0$ the instability may grow in time. Nevertheless, in our computer calculations, we find that either the excited low or high frequency modes have always finite damping rates. In addition, the plasma density gradient near the edge is very large and so is the mismatch between the waves, which make very difficult the excitation of temporally growing modes [7-9]. It should also be noted that the damping rates will, in this case, depress more the instability than they do when $sgn(v_{1\xi} v_{2\xi}) > 0$. This is because they add up their contributions which yields larger values of λ_D; if $\lambda_D \geq 2|\Lambda_0|$, the instability cannot grow either in time or in space. Hence, we shall not consider this case any further.

The angle ϕ is to be chosen such that the amplification factor is maximal with respect to $\cos(\phi) = v_{1x}/v_{1\perp}$. The level of growth of the instability is basically governed by $|\Lambda_0 L|$; the mismatch and damping rates reduce this level, but their strength are most dependent on the plasma density gradient and on the parallel refractive indices of the excited waves, respectively . Hence, we require that $|\Lambda_0 L|$ to be maximized with respect to $\cos(\phi)$. By using the definitions of L and $|\Lambda_0|$ we find, $|\Lambda_0 L| = - |\gamma_0| / \sqrt{|v_{1\bar{x}} v_{2x}|}\, v_{0\perp}/v_{0z}\, w$. The dependences on ϕ are given by $|\gamma_0|$ which goes like $\sin(\phi)$ (see Eq. (12a)), by $v_{1\bar{x}}$ which is

$$v_{1\bar{x}} = -v_{1x} [- \cos(\phi) \frac{v_{1\perp}}{v_{1x}} + \frac{v_{0\perp}}{v_{0z}}],$$

and by v_{2x} which is proportional to $(1 - k_{1\perp}^2 / k_{2\perp}^2 \sin^2(\phi))^{1/2}$. The angle that maximizes $|\Lambda_0 L|$, satisfy the equation

$$2 \cos(\phi) [- \frac{v_{1x}}{v_{1\perp}} + \frac{v_{0z}}{v_{0\perp}} \cos(\phi)] + \frac{v_{0z}}{v_{0\perp}} \sin^2(\phi) [1 - \frac{k_{1\perp}^2}{k_{2\perp}^2} \sin^2(\phi)] = 0 \tag{19a}$$

For the low frequency mode to propagate in the plasma, we require that $k_{1\perp}^2/k_{2\perp}^2 \sin^2(\phi)$ to be much smaller than one, allowing us to neglect this term in the Eq. (19a). Solving for the maximum ϕ, we find

$$\cos(\phi_m) = \frac{v_{1z}v_{0\perp}}{v_{1\perp}v_{0z}} - [(\frac{v_{1z}v_{0\perp}}{v_{1\perp}v_{0z}})^2 - 1]^{1/2}. \tag{19b}$$

Note that as $\cos(\phi_m) > 0$ we have that $\mathrm{sgn}(v_{1x}v_{1z}) < 0$ and, then, that $\mathrm{sgn}(v_{1x}v_{2x}) < 0$. In the calculations, we shall only consider the angle ϕ_m.

Putting together Eqs. (6), (8), (12a), and (19b), we find

$$|\lambda_0 L| = \frac{E_0\,\omega_{\ell h}\,w\,v_{0\perp}\,v_{1z}}{2\sqrt{2}\,B_0\,c_s\,v_{Te}\,v_{0z}\,v_{1\perp}} \left(\frac{\sqrt{2}\,|k_{2z}|\,v_{Te}}{\omega_2} \frac{v_{Te}\,T_i\,\Omega_i^2\,\omega_1}{|v_{1z}\,R\,k_{2x}|\,T_e\,\omega_0^2\,v_{Ti}}\right)^{1/2}$$

$$\times\left(-\frac{v_{0\perp}}{v_{0z}} - (\frac{v_{0\perp}^2}{v_{0z}^2} - \frac{v_{1\perp}^2}{v_{1z}^2})^{1/2}\right)^{1/2} \left(1 + \frac{\omega_2}{\sqrt{2}\,|k_{2z}|\,v_{Te}}\,Z_R(\frac{\omega_2}{\sqrt{2}\,|k_{2z}|\,v_{Te}})\right). \tag{20}$$

We remark that because $|\lambda_0|$ is proportional to $v_{1z}^{-1/2}$, the amplification factor will be the largest for the largest possibles n_{1z}. Also, $|\lambda_0 L|$ increases linearly with increasing central density n_0, and decreases linearly with increasing pump frequency ω_0. This, we shall see, will have important consequences to decide whether the resonant parametric decay will occur or will not.

Substituting Eq. (19b) into the definition of ρ after Eq. (13), we get

$$\rho = (1 - \frac{v_{2x}}{v_{1x}}) \frac{1 - [1 - (\frac{v_{0z}\,v_{1\perp}}{v_{1z}\,v_{0\perp}})^2]^{1/2}}{(1 - v_{2x}/v_{1x})\left(1 - [1 - (\frac{v_{0z}\,v_{1\perp}}{v_{1z}\,v_{0\perp}})^2]^{1/2}\right) - 1}. \tag{21a}$$

In the computer calculations we find that v_{2x} is always much smaller than v_{1x}, which allows us to approximate ρ by $1 - [1 - (v_{0z}v_{1\perp}/v_{1z}v_{1\perp})^2]^{-1/2}$. The distance L is now approximately given by,

$$L = |\rho\,\frac{v_{0x}}{v_{0z}}|\,w \simeq \frac{v_{0x}}{v_{0z}}\left([1 - (\frac{v_{0z}v_{1\perp}}{v_{0\perp}v_{1z}})^2]^{-1/2} - 1\right) w. \tag{21b}$$

Note that L increases linearly with pump frequency and so does $K'L$.

In terms of the sideband and pump group velocities at each of the extremes of the pump cone $\xi = \pm L/2$, we find

$$\frac{K' L}{k_{0z}} = - \frac{v_{0z}(L/2)}{v_{0\perp}(L/2)} + \frac{v_{0z}(-L/2)}{v_{0\perp}(-L/2)} - \left(- \frac{v_{1z}(L/2)}{v_{1\perp}(L/2)} + \frac{v_{1z}(-L/2)}{v_{1\perp}(-L/2)} \right) \frac{n_{1z}\,\omega_1}{n_{0z}\,\omega_0} \cos(\phi_m) \qquad (22)$$

where the components of the group velocities are evaluated at the local densities, $n(\pm L/2) = n_0 \pm |\nabla n|\, L/2$. We shall always assume that $n(-L/2) \geq 10^{11}$ cm^{-3}; if L is large enough so that $n(\xi)$ becomes smaller than 10^{11} cm^{-3} at a certain ξ_0, we shall assume that the density profile flattens for $\xi < \xi_0$ at the minimum density 10^{11} cm^{-3}.

IV. RESULTS AND CONCLUSIONS

We shall proceed in our calculations by assuming plasma edge parameters consistent with measurements on the JFT2 heating experiment. We consider a hydrogen plasma and take the plasma temperatures and toroidal magnetic field to be spatially homogeneous; their values are, T_e = 20 ev, T_i = 8 ev, B_0 = 15 kG. The plasma density will be assumed to obey the profile given in Eq. (15a), where n_0 will be either 5 x 10^{11} cm^{-3} or 10^{12} cm^{-3}; the corresponding density gradients are $|\nabla n|$ = 5 x 10^{12} cm^{-4} and 10^{13} cm^{-4}. The half-width of the plasma slab is equal to the tokamak minor radius, i.e., r = 25 cm. The applied Rf-power is P_0 = 150 kW, driven at the plasma wall through a four-waveguides array, each of width $w/4$ = 1.4 cm, and height h = 29 cm. The pump frequency will vary between 715 to 1000 Mhz. We restrict ourselves to the propagation cone $k_{0z} > 0$. The parallel refractive index of the pump field n_{0z} is taken according to the linear theory [13] and depends on the pump frequency; it ranges between 5.35 to 3.85. The accessible n_z is 1.9, and we assume that all the input Rf-power is accessible in the plasma.

In the figures we present next we plot the amplification factor Γ, as given by Eqs. (18), versus the parallel refractive index n_{1z} of the excited high frequency wave, for given values of p and pump frequency. We notice that n_{1z} as given in Eq. (10), is a function of ω_2/ω_0, n_{0z} and of the free parameter $\omega_2/(|k_{2z}|v_{Te})$; this is ranging between 4 v_{Ti}/v_{Te} and, say, 0.75. The frequency ω_2 is chosen as indicated in Sec. IIA, i.e., it satifies the dispersion relation Eq. (3) and minimizes the damping rate of the low frequency mode. In Figs. 2 and 3, we consider two different cases depending on wether the high frequency excited wave is moving toward the center of the plasma, i.e., $v_{1x} < 0$, (case A), or toward the edge, i.e., $v_{1x} > 0$ (case B). The low frequency mode moves in opposite direction to the high frequency one, i.e., we always have that $sgn(v_{1x}v_{2x}) < 0$.

In Fig. 2, we assume that n_0 = 5 x 10^{11} cm^{-3}, $|\nabla n|$ = 5 x 10^{12} cm^{-4}, and ω_0 = 715 Mhz ($\omega_0 \simeq 45\ \Omega_i$). We consider the excitation of the first fifth cyclotron harmonics; the numbers on the different curves indicate the order of the excited cyclotron waves. Let us first study Fig. 2A.

Comparing the curves that correspond to the excitation of the different modes, we observe that from $p = 1$ through $p = 3$ the amplification factor increases with increasing p. At $p = 3$, it saturates and starts decreasing with increasing p; cyclotron harmonic waves with p greater than 5 are not excited. This can be explained in terms of Eq. (10), that we rewrite here assuming that $\omega_2/k_{2z} < 0$ and keeping only the relevant contributions,

$$\frac{\omega_1}{k_{1z}v_{Te}} = \frac{\omega_2/(|k_{2z}|v_{Te})}{\frac{\omega_2/|k_{2z}|v_{Te}}{\omega_0/k_{0z}v_{Te}} + \omega_2/\omega_0}.$$

The largest values of n_{1z} are always reached for small values of $\omega_2/|k_{2z}|$. For fixed $\omega_2/|k_{2z}|$, n_{1z} increases with increasing ω_2; this is because the denominator increases with increasing p. As we have already commented in Sec. III, the larger n_{1z} the larger $|\Lambda_0 L|$. On the other hand if n_{1z} becomes greater than 40 or 50, the excited high frequency wave will be strongly damped by electrons, which will prevent the resonant decay. As $\omega_2/|k_{2z}|$ increases, the Landau damping rate of the low mode due to electrons will increase too. In addition, for small $\omega_2/|k_{2z}|$ the argument of the Z-function in the denominator of the dispersion relation Eq. (3) has to be close to one in order to solve it for a real $k_{2\perp}$ which will, in turn, increase the rate of ion-cyclotron harmonic damping; this effect becomes more appreciable for the largest p. The most favorable combination of all these constraints selects which are the dominant harmonics to be excited and, for given harmonic, which are the values of n_{1z} that are excited.

For $p = 1$ and for small values of $\omega_2/|k_{2z}|$ so that the ion-cyclotron wave is not damped by electrons, the corresponding n_{1z} can be large enough to generate moderate values of $|\Lambda_0 L|$. Increasing $\omega_2/|k_{2z}|$, n_{1z} decreases and so does $|\Lambda_0 L|$. For $p = 5$ and small values of $\omega_2/|k_{2z}|$, electron Landau damping for the high frequency wave and ion-cyclotron damping for the low mode can be very large. Thus, there are optimum values of p, such as $p = 2,3$, for which the combination of these effects compromise so that to allow for the strongest resonant excitation to occur.

In Fig. 2B, we represent Γ for the same plasma parameters as in Fig. 2A, but now $\omega_2/k_{2z} > 0$, and $n_{1z} < 0$. For fixed $\omega_2/|k_{2z}|$, the excited n_{1z} as given by Eq. (10), are always smaller in magnitude than those excited in case of Fig. 2A, which may explain why Γ is now slightly smaller.

It is also important to notice that, in general, L is always quite large (greater than or of the order of 2 cm) and it is the largest for the smallest p. Thus, when $p = 1$ or 2, the instability saturates before it can reach the extremes of the pump cone. As p becomes greater than or equal to 3, L becomes smaller and the instability may amplify in the entire pump interval L. In Table I, we present, for the case of Fig. 2, the characteristics of the excited modes which maximize amplification, in terms of parameters which determine their Landau damping rates. We observe that the damping rates of the excited waves increase by increasing the order of the excited harmonics for both electron and ion damping.

In Fig. 3, we assume that $\omega_0 = 900$ Mhz; other plasma parameters are as in Fig. 2. Because $|\Lambda_0 L|$ is proportional to the pump electric field E_0 which is given in Eq. (12b), and this decreases linearly with increasing pump frequency, the amplification factor also decreases as ω_0 increases. Also, notice that for fixed $\omega_2/|k_{2z}|$, n_{1z} decreases linearly with increasing ω_0. As ω_0 becomes larger than 1 Ghz, Γ goes to zero for any value of p. Table II contains the main characteristics of the excited modes which maximize amplification.

In Fig. 4, we take $n_0 = 10^{12}$ cm^{-3}, $|\Delta n| = 10^{13}$ cm^{-4}, and $\omega_0 = 1$ Ghz. We present only the case $n_{1z} > 0$ which, as we already know, always gives the largest values of Γ. We want to illustrate that the excitation of the cyclotron harmonic waves are also dependent on central plasma density n_0; this is because E_0 increases linearly with increasing n_0. The pump frequency range for which the cyclotron harmonic waves are now excited is different from the case in Figs. 2 and 3. The reason why for $p = 1$ the curve is suddenly cut at $n_{1z} \simeq 35$ is because $k_{1\perp}^2/k_{2\perp}^2 \sin^2(\phi_m)$ is larger than or equal to one (i.e., $k_{2x} \simeq 0$), and the corresponding ion-cyclotron wave cannot propagate in the plasma. When ω_0 is larger than 1.2 Ghz we find that Γ is zero for any p. The characteristics of the strongest excited cyclotron waves are very similar to the ones presented in Tables I and II, and the general scaling of the damping rates with respect to the excited p is the same.

In Fig. 5, ω_0 is 900 Mhz for case A, and 825 Mhz for case B; other plasma parameters are as in Fig. 4. We observe that there are a maximum of six ion-cyclotron harmonics excited.

Comparing cases A and B we also observe that higher n_{1z} are excited decreasing the pump frequency. The most remarkable feature of this figure is the behavior of Γ for the first excited cyclotron harmonic $p = 1$ with respect to n_{1z}. We see that for $n_{1z} \geq 25$ the amplification factor becomes very large, larger than for any other excited harmonics. This is because $k_{2x} \simeq 0$, which leads to singular values of $|\Lambda_0 L|$ as given by Eq. (20); note also that this effect becomes even more noticeable as ω_0 decreases. If $\omega_0 \leq 715$ Mhz other excited modes such as $p = 2$, can also experience the same singular behaviour.

We have already commented that for fixed n_0, decreasing the pump frequency leads to higher excited n_{1z}. As n_{1z} increases $k_{1\perp}^2/k_{2\perp}^2 \sin^2(\phi_m)$ gets closer to one or, what is equivalent, k_{2x} gets closer to zero; (we can always make $\sin^2(\phi)$ smaller so that k_{2x} becomes larger, but then γ_0 and the amplification factor will go to zero.) Also, $k_{2\perp}$ as given in Eq. (3) increases with increasing p which implies that higher n_{1z} are required (i.e., smaller values of ω_0) to make $k_{2x} \simeq 0$ as the number of the excited harmonic p increases. If n_{1z} and p are such that $k_{2x}^2 \leq 0$ then these modes cannot be resonantly excited. This is responsible for the suddenly cut of the curves $p = 1$ in Fig. 5, for $n_{1z} \geq 40$. Our formulation is not valid when this happens and such large values of Γ are not reliable. In fact, since the resonant matching conditions for the perpendicular components of the wavenumbers are responsible for the negative or small values of k_{2x}^2, when this happens, we should formulate the parametric decay assuming that the low frequency mode is non-resonant (i.e., it is a quasi-mode) [2]. This means that the wavenumber of the low frequency quasi-mode is to be chosen at any point in the plasma such that it matches the wavenumbers of the lower-hybrid waves. This figure illustrates that the non-resonant decay can also be very important. Because higher n_{1z} may be excited via quasi-mode decay, it can be expected that a larger amount of the input power may be deposited near the plasma edge. We remark that this effect can also be observed decreasing ω_0 below 715 Mhz, in the cases of Figs. 2 and 3.

Let us now make some final remarks on the scaling of Γ with respect to the input power density, for fixed values of n_0 and ω_0. By increasing the amount of power, E_0 increases and so does $|\Lambda_0 L|$. This will mean that the amplification factor Γ will also become larger. However, it can also be

expected that because of this, higher n_{1z} will be excited via non-resonant decay in a similar way as it was explained in the case of Fig. 5. (The highest is n_{1z} the closet is k_{2x}^2 to become negative, which will eventually make impossible the resonant decay.) These high n_{1z} will deposit a certain amount of the power directly on the electrons via linear Landau damping. This, in turn, means that the power which is left and which may parametrically decay via resonant ion-cyclotron excitations, will not be as much as the input power at the plasma wall. Thus, the amplification factor and, subsequently, the amplitude of the resonantly excited modes, is expected eventually to saturate as the input Rf-power is increased. But this does not necessarily imply that the Rf-power is getting in the plasma center since it might have been deposited near the edge through the excitation of high n_{1z} via quasi-mode decay.

In summary, we have presented calculations for the parametric excitation of ion-cyclotron harmonic waves driven by lower-hybrid pump electric field near the plasma edge. It is shown that the excitation of these modes is critically dependent on pump frequency and on plasma density. The ion-cyclotron waves are shown to have a finite damping rate. The parallel refractive index of the excited sideband field is found to be much larger than that of the driven pump field. Transition to quasi-mode excitations may occur for small values of ω_0 or large values of P_0. All this suggests that appreciable amount of the input Rf-power is deposited near the plasma edge.

APPENDIX

Let us assume that $|\lambda_0|^2 \gg |d\Delta k/d\xi|$ and take $\mathrm{sgn}(v_{1\xi}v_{2\xi}) > 0$. By eliminating $\hat{a}_2$ from Eq. (17a) we obtain

$$\frac{d^2\hat{a}_1}{d\xi^2} - [|\lambda_0|^2 + \frac{1}{4}\beta^2(\xi)]\hat{a}_1 = b\,\delta(\xi). \tag{A.1}$$

The Dirac delta function in the right-hand side, has been introduced to take into account the presence of the thermal fluctuations which initiates the parametric decay; b is the level of the thermal source ($b \ll a_0$).

We next define a new complex variable,

$$z = \frac{\lambda_D + iK'\xi}{2|\lambda_0|}. \tag{A.2}$$

Within the WKB approximation two independent solutions to the homogeneous equation (A.1) are,

$$\psi_\pm(z) = \frac{1}{\sqrt{\zeta(z)}} \exp[\pm i \frac{2|\lambda_0|^2}{K'} \int_{\pm i}^{z} (1 + z'^2)^{1/2}\, dz'] \tag{A.3}$$

where $\zeta(z) = |\lambda_0|(1 + z^2)^{1/2}$; the pump boundary limits ($\xi = \pm L/2$) in the complex variable z are c and c^*. Let us call r and r^*, the points where the line $\mathrm{Re}(z) = \lambda_D/2|\lambda_0|$ intersects the anti-Stokes lines,

$$\mathrm{Im}[\int_{\pm i}^{z} (1 + z'^2)^{1/2} dz'] = 0. \tag{A.4}$$

The amplitudes of the solutions $\psi_\pm$ are exponentially large for $|\mathrm{Im}(z)| < \mathrm{Im}(r)$. As $\mathrm{Im}(z)$ becomes larger than $\mathrm{Im}(r)$, ψ_+ becomes exponentially small. As $\mathrm{Im}(z)$ becomes smaller than $\mathrm{Im}(r^*)$ then it is ψ_- the one that is exponentially small.

The solution to the inhomogeneous equation (A.1) has to be such that it decreases in magnitude as $|\mathrm{Im}(z)|$ becomes larger than $\mathrm{Im}(r)$. Thus, it must be proportional to ψ_+, for $\mathrm{Im}(z)$

greater than zero, and proportional to ψ_- for Im(z) smaller than zero. These two functions must match smoothly at $\xi = 0$, but their first derivatives need not. The discontinuity in the derivative is given by the level of the thermal source. The solution to Eq. (A.1) that satisfy these boundary conditions is found to be

$$\hat{a}_1(z) = \frac{b}{\psi_+'(z_0)\psi_-(z_0) - \psi_+(z_0)\psi_-'(z_0)} \left[\vartheta(z - z_0)\,\psi_-(z_0)\,\psi_+(z) + \vartheta(z_0 - z)\,\psi_+(z_0)\,\psi_-(z)\right] \quad (A.5)$$

where $z_0 = \lambda_D/2|\lambda_0|$, $\mathrm{Re}(z) = z_0$, $\psi_\pm'(z_0)$ denotes differentiation with respect to z evaluated at $z = z_0$, and $\vartheta(z - z_0)$ is the unit step function which is zero for $\xi < 0$. The amplification factor can be obtained from Eq. (A.5) and it is as presented in Eqs. (18).

Acknowledgments

The author gratefully acknowledges Prof. A. Bers for encouraging this investigation. This work has been supported by the U.S. Department of Energy Contract (ET78-S-02-4682).

References

1. Porkolab, M., Phys. Fluids 17 (1974) 1432.

   Porkolab, M., Phys. Fluids 20 (1977) 2058.

2. Villalón, E., Bers, A., Nucl. Fusion 20 (1980) 243.

3. Tripathi, V. K., Liu, C. S., Grebogi, C., Phys. Fluids 22 (1979) 301.

4. Berger, R. L., Perkins, F. W., Phys. Fluids 19 (1976) 406.

5. Imai, T., Nagashima, T., Yamamoto, T., Uehara, K., Konoshima, S., et al, Phys. Rev. Lett. 43 (1979) 586.

6. Bernabei, S., Daugnney, C., Hooke, W., Motley, R., Nagashima, T., et al, in Third Symposium on Plasma Heating in Toroidal Devices, Editrice Compositore-Bologna, Italy, (1976) 68.

   Gormezano, C., Blanc, P., Durvaux, M., Hess, W., Ichtchenko, G., et al, in Third Topical Conference on Radio Frequency Plasma Heating, California Institute of Technology, Pasadena, California, U.S.A., (1978) A3-1

   Singh, C. M., Briand, P., Dupas, L., Grelot, P., in Plasma Physics (Proc. Int. Conf.) Vol. 1, Fusion Research Association of Japan, Nagoya, Japan , (1980) 321.

   Knowlton, K., Luckhardt, S. C., Porkolab, M., in Plasma Physics (Proc. Int. Conf.) Vol. 1, Fusion Research Association of Japan, Nagoya, Japan , (1980) 318.

7. Rosenbluth, M. N., Phys. Rev. Lett. 29 (1972) 565.

8. White, R., Kaw, P., Pesme, D., Rosenbluth, M. N., Laval, G., Huff, R., Varma, R., Nucl.

Fusion 14 (1974) 45.

9. Villalón, E., Resonant Parametric Excitation Driven by Lower hybrid Fields, Massachusetts Institute of Technology. Plasma Fusion Center Rep. JA-80-2 (to be published in Phys. Fluids).

10. Bers, A., in Plasma Physics-Les Houches, Gordon and Breach, New York, (1975) 205.

11. Reiman, A., Phys. Fluids 21 (1978) 1000.

12. Bobroff, D. L., J. Appl. Phys. 36 (1965) 1760.

13. Brambilla, M., Nucl. Fusion 16 (1976) 47.

FIGURE CAPTIONS

Figure 1. Pump propagation cone and trajectory of the pulse response. The coordinates (x, z) lie along the direction of the plasma inhomogeneities and toroidal magnetic field, respectively. The cordinates $(\bar{x}, \bar{z})$ lie along and perpendicular to the pump propagation cone. The line of the pulse response is $\bar{z} - \alpha\bar{x} = z_f$, with z_f a free parameter defining where in the plasma the resonant interaction is taking place.

Figure 2. Amplification factor versus sideband parallel refractive index. The numbers on the different curves indicate the order of the excited cyclotron harmonic. We assume $n_0 = 5 \times 10^{11}$ cm^{-3}, $|\nabla n| = 5 \times 10^{12}$ cm^{-4}, $\omega_0 = 715$ Mhz, $n_{0z} = 5.35$, $P_0 = 150$ kW. A) $v_{1x} < 0$, $v_{2x} > 0$; B) $v_{1x} > 0$, $v_{2x} < 0$.

Figure 3. Amplification factor versus sideband parallel refractive index. The numbers on the different curves indicate the order of the excited cyclotron harmonic. We assume $n_0 = 5 \times 10^{11}$ cm^{-3}, $|\nabla n| = 5 \times 10^{12}$ cm^{-4}, $\omega_0 = 900$ Mhz, $n_{0z} = 4.25$, $P_0 = 150$ kW. A) $v_{1x} < 0$, $v_{2x} > 0$; B) $v_{1x} > 0$, $v_{2x} < 0$.

Figure 4. Amplification factor versus sideband parallel refractive index. The numbers on the different curves indicate the order of the excited cyclotron harmonic. We assume $n_0 = 10^{12}$ cm^{-3}, $|\nabla n| = 10^{13}$ cm^{-4}, $\omega_0 = 1$ Ghz, $n_{0z} = 3.85$, $P_0 = 150$ kW.

Figure 4. Amplification factor versus sideband parallel refractive index. The numbers on the different curves indicate the order of the excited cyclotron harmonic. We assume $n_0 = 10^{12}$ cm^{-3}, $|\nabla n| = 10^{13}$ cm^{-4}, $P_0 = 150$ kW. A) $\omega_0 = 900$ Mhz, $n_{0z} = 4.25$; B) $\omega_0 = 825$ Mhz, $n_{0z} = 4.65$.

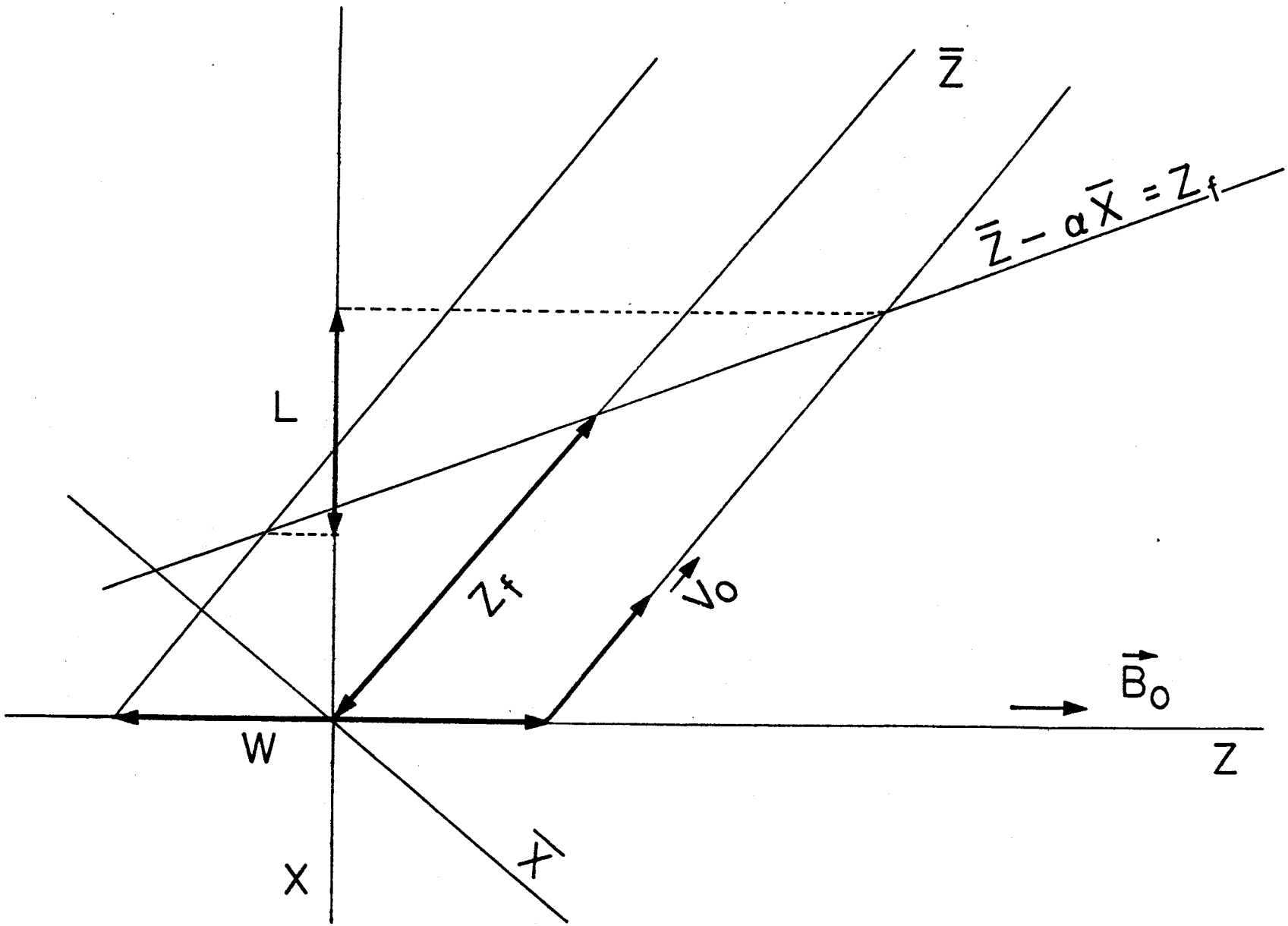

FIGURE 1

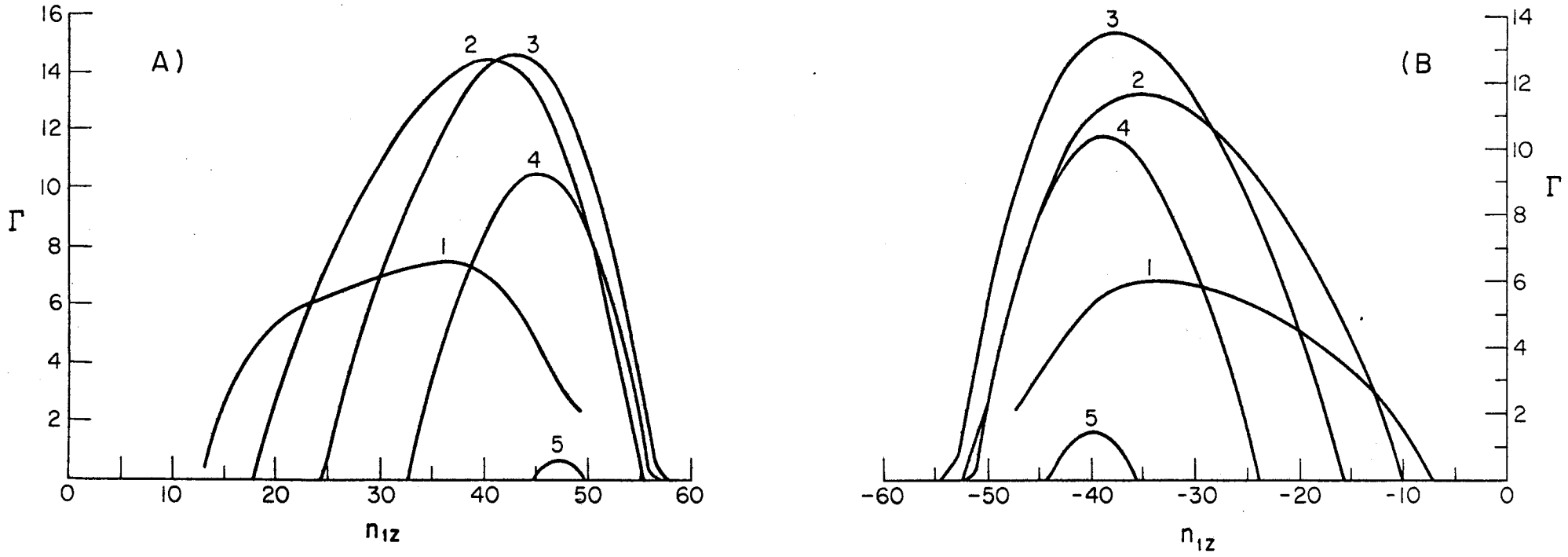

FIGURE 2

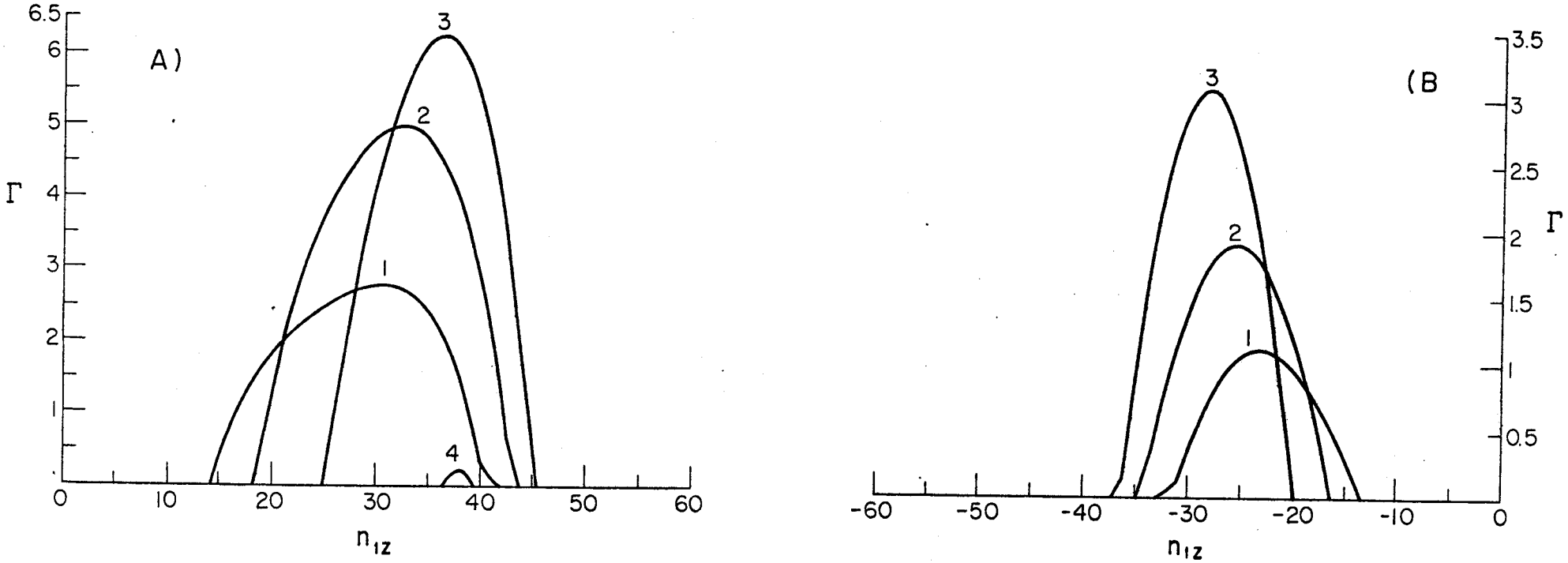
A)
(B
Γ
n_{1z}
6.5
6
5
4
3
2
1
0
10
20
30
40
50
60
-60
-50
-40
-30
-20
-10
3.5
3
2.5
2
1.5
1
0.5

FIGURE 3

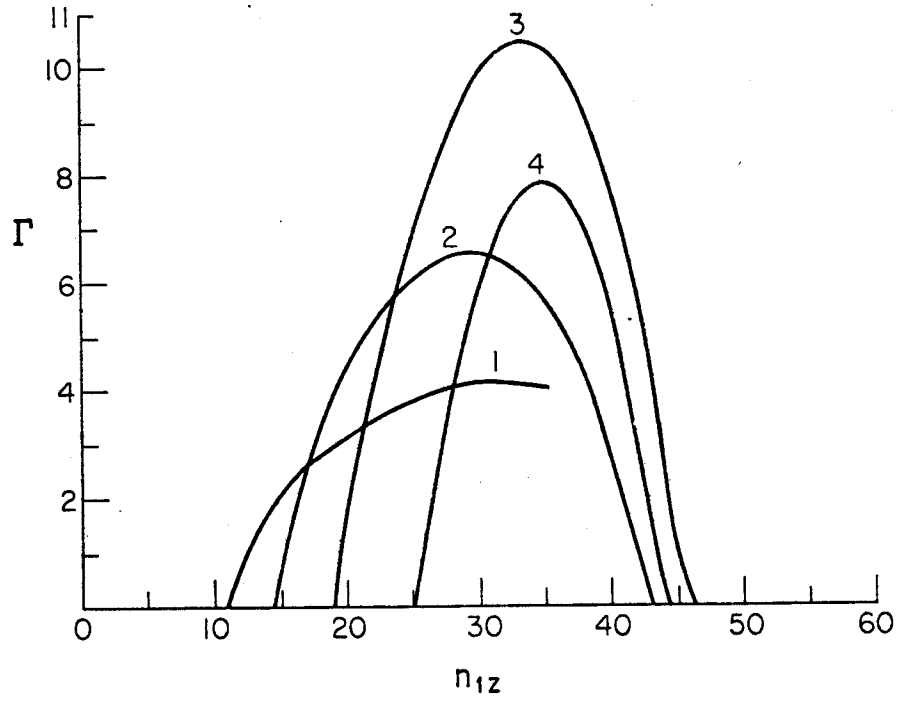

FIGURE 4

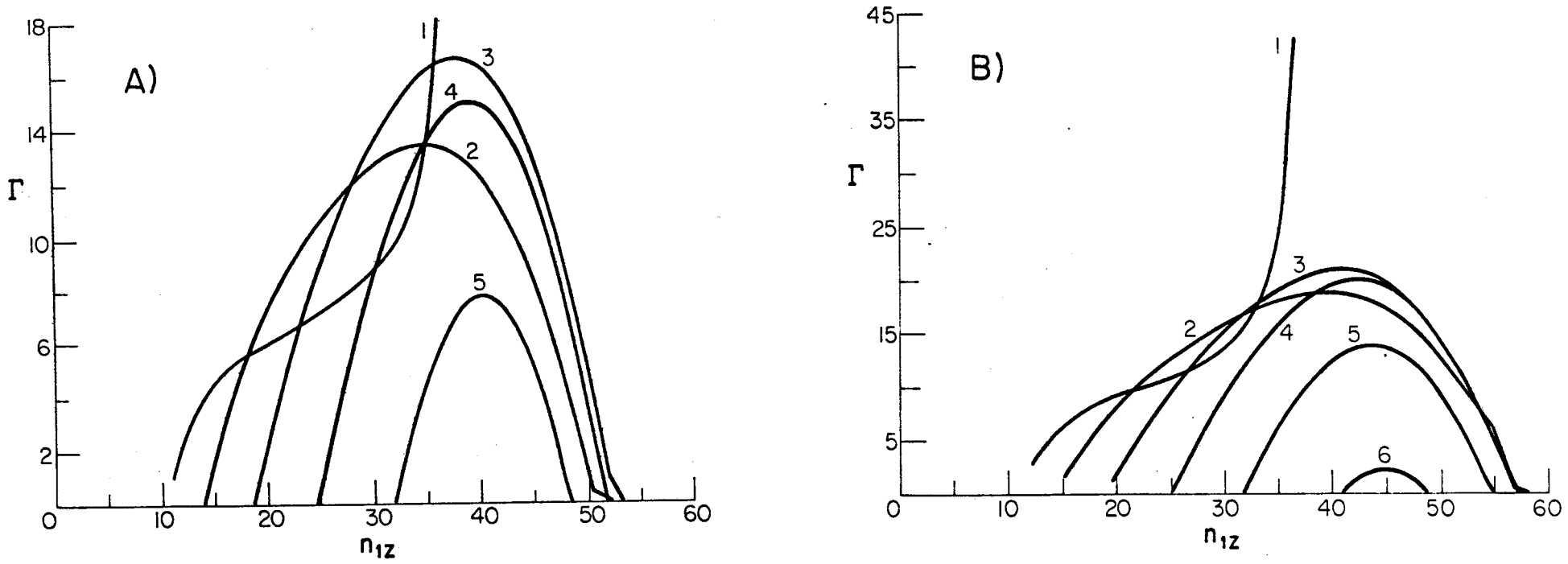

FIGURE 5

TABLE I. CHARACTERISTICS OF THE ION CYCLOTRON MODE WHICH MAXIMIZES AMPLIFICATION, FOR THE CASE OF FIGURE 2.

	P	$\frac{\omega_2}{\Omega i}$	$\frac{\omega_2}{k_{2z} V_{Te}}$	$\frac{\omega_2 - p\Omega i}{\lvert k_{2z}\rvert V_{Ti}}$	$\frac{\omega_1}{k_{1z} V_{Te}}$
A)	1	1.53	-0.16	3.74	4.40
	2	2.48	-0.26	3.41	4.00
	3	3.47	-0.34	3.16	3.72
	4	4.47	-0.43	3.07	3.55
	5	5.48	-0.51	3.03	3.40
B)	1	1.55	0.14	3.41	-4.88
	2	2.50	0.22	3.03	-4.58
	3	3.49	0.30	2.83	-4.26
	4	4.49	0.38	2.77	-4.11
	5	5.49	0.46	2.78	-4.03

TABLE II. CHARACTERISTICS OF THE ION CYCLOTRON MODE WHICH MAXIMIZES AMPLIFICATION, FOR THE CASE OF FIGURE 3.

	P	$\frac{\omega_2}{\Omega i}$	$\frac{\omega_2}{k_{2z} V_{Te}}$	$\frac{\omega_2 - p\Omega i}{\lvert k_{2z} \rvert V_{Ti}}$	$\frac{\omega_1}{k_{1z} V_{Te}}$
A)	1	1.52	-0.17	3.85	5.31
	2	2.48	-0.25	3.35	4.95
	3	3.48	-0.32	3.00	4.44
	4	4.48	-0.40	2.89	4.23
B)	1	1.54	0.15	3.63	-6.81
	2	2.50	0.23	3.15	-6.21
	3	3.49	0.31	2.91	-5.67